PHYSICAL REVIEW B **113**, 134438 (2026)

Magnetic and phononic dynamics in the two-ladder quantum magnet $(C_5H_9NH_3)_2CuBr_4$

J. Philippe,[1,2] F. Elson,[3] T. Arh,[1] S. Sanz,[4] M. Metzelaars,[4,5] D. W. Tam,[3] O. K. Forslund,[2,6] O. Shliakhtun,[1,2]
C. Jiang,[3] J. Lass,[1] M. D. Le,[7] J. Ollivier,[8] P. Bouillot,[9] T. Giamarchi,[9] M. Bartkowiak,[1] D. G. Mazzone,[1]
P. Kögerler,[5] M. Månsson,[3] A. M. Läuchli,[10,11] Y. Sassa,[3,12] M. Janoschek,[1,2] B. Normand,[10] and G. Simutis[1,12,*]

[1] *PSI Center for Neutron and Muon Sciences, CH-5232 Villigen-PSI, Switzerland*
[2] *Physik-Institut, Universität Zürich, Winterthurerstrasse 190, CH-8057 Zürich, Switzerland*
[3] *Department of Applied Physics, KTH Royal Institute of Technology, SE-106 91 Stockholm, Sweden*
[4] *Peter Grünberg Institute, Electronic Properties (PGI-6), Forschungszentrum Jülich, 52425 Jülich, Germany*
[5] *Institute of Inorganic Chemistry, RWTH Aachen University, 52056 Aachen, Germany*
[6] *Department of Physics and Astronomy, Uppsala University, Box 516, SE-751 20 Uppsala, Sweden*
[7] *ISIS facility, Rutherford Appleton Laboratory, Chilton, Didcot OX11 0QX Oxfordshire, United Kingdom*
[8] *Institut Laue Langevin, BP156, 38042 Grenoble, France*
[9] *Department of Quantum Matter Physics, University of Geneva, Quai Ernest-Ansermet 24, CH-1211 Geneva, Switzerland*
[10] *PSI Center for Scientific Computing, Theory and Data, CH-5232 Villigen-PSI, Switzerland*
[11] *Institute of Physics, Ecole Polytechnique Fédérale de Lausanne (EPFL), CH-1015 Lausanne, Switzerland*
[12] *Department of Physics, Chalmers University of Technology, SE-412 96 Göteborg, Sweden*

(Received 24 October 2025; revised 2 March 2026; accepted 10 March 2026; published 22 April 2026)

In quantum magnetic materials it is common to observe both static and dynamic lattice effects on the magnetic excitation spectrum. Less common is to find that the magnetic correlations have a significant impact on the phonon spectrum. Here we study the metal-organic material $(C_5H_9NH_3)_2CuBr_4$(Cu-CPA), in which an explanation of the low-lying excitations depends crucially on a full understanding of both the spin and lattice subsystems. We report high-resolution neutron spectroscopy enabled by large, deuterated single crystals that reveal how both sectors are affected by the recently discovered structural phase transition. By measuring over several Brillouin zones, we disentangle the vibrational contribution to the spectrum in order to obtain an accurate estimate of the quasi-one-dimensional magnetic signal. The low-energy magnetic excitations are dominated by two gaps, $\Delta_b = 0.41$ meV and $\Delta_a = 0.55$ meV, which contribute with equal intensity ratios, confirming that Cu-CPA realizes a two-ladder spin Hamiltonian, and we deduce the magnetic interaction parameters of both ladders. The phonon spectrum contains highly localized modes at an anomalously low energy around 2 meV. For half of these modes, this characteristic frequency drops by approximately 5% as magnetic correlations become established with decreasing temperature, and we connect this apparent "elastomagnetic" behavior with the location and structure of the cyclopentylammonium rings.

DOI: 10.1103/89j6-f5zx

I. INTRODUCTION

Insulating materials formed from magnetic ions with spin $S = 1/2$ create an excellent platform for the experimental study of many-body quantum physics. Because these materials have only a small number of well-defined and short-ranged interactions, they can realize paradigmatic low-dimensional spin models whose analysis was once the province only of mathematical physics. This is particularly true in one-dimensional (1D) systems, whose gapless phases can realize integrable models and quantum field theories [1]. In addition to nearest-neighbor spin chains of Heisenberg, Ising, or XY type, 1D models with more than one parameter include alternating chains and chains with next- or further-neighbor interactions, as well as quantum spin ladders [2,3]. Two-leg ladders form a class of quantum systems whose field-induced ground states and excitation spectra are controlled by a single parameter, the interaction ratio $\alpha = J_{\text{leg}}/J_{\text{rung}}$ [4].

Early spin-ladder compounds were based on cuprates [5–11] and hence had the two properties that $\alpha \approx 1$ and the interaction parameters were well over 100 meV, placing them far outside the range of laboratory magnetic fields. Metal-organic materials with a wide variety of ligands provided both geometrical flexibility and, because of the large organic spacer groups, the possibility of very small interaction parameters (meaning in the 1 meV range or truly vanishing [12]). Several early metal-organic spin ladders, most notably $(C_5H_{12}N)_2CuBr_4$ (BPCB) and $(C_5H_{12}N)_2CuCl_4$ (BPCC) [13,14], realized the strong-rung regime (small α) and therefore could be described very well by bond-operator

---

[*] Contact author: gediminas.simutis@psi.ch

methods, both in their gapped phases [15] and in their field-induced gapless ones [16–18]. Strong-leg ladders have turned out to be less common, and to date only the compound $(C_7H_{10}N_2)_2CuBr_4$ (DIMPY) has been studied in detail in experiment [19–21], while numerical methods based on exact diagonalization (ED) and matrix-product states (MPS) have allowed the unbiased numerical calculation of complete excitation spectra at all α and all applied magnetic fields [4,22].

The phonon contribution to the excitation spectrum of metal-organic magnets has to date been treated in the same way as inorganic materials, meaning that no optical phonons are expected at 1 meV energies and the thermodynamic contributions from lattice excitations have been modeled using the Debye form. However, important properties of phonons in metal-organic frameworks are first that their energies can be rather low, due to the presence of large organic groups, and second that these groups can host many near-degenerate and low-lying phonon modes. Although certain anomalies persist in the body of experimental data on materials such as DIMPY [23], the possibility of a connection with such phonons has yet to be considered.

Here we investigate a metal-organic spin-ladder compound, Bis(cyclopentylammonium)tetrabromocuprate $[(C_5H_9NH_3)_2CuBr_4$ or $(CPA)_2CuBr_4$, which we abbreviate Cu-CPA] [12], in which a detailed consideration of the phonon contribution is integral to the complete understanding of the low-energy spectrum. Cu-CPA was identified initially as a strong-leg spin ladder [12], based on magnetic susceptibility and x-ray diffraction measurements performed on powder samples. However, it was discovered recently that Cu-CPA undergoes an order-disorder transition in the structure of one CPA ring at 136 K (132 K in the deuterated analog) and a structural phase transition at 113 K (119 K), the latter splitting the magnetic contribution into equally weighted components arising from two inequivalent spin ladders [24]. These transitions reflect the presence of multiple low-lying optical phonons in Cu-CPA that can make significant contributions to the spectral and thermodynamic properties.

The structure of this article is as follows. In Sec. II we introduce the structural properties of $(C_5H_9NH_3)_2CuBr_4$ and their consequences for thermodynamic measurements made to date. In Sec. III we describe our inelastic neutron scattering (INS) measurements, the analysis by which we achieve an unambiguous separation of the magnetic and lattice contributions, and our determination of the magnetic interaction parameters of both ladders. In Sec. IV we reanalyze the specific-heat data of Cu-CPA to identify the full phonon contribution. In Sec. V we discuss the physical origin of the anomalous low-energy phononic properties and the candidate mechanisms for the clear effects of strong magnetic correlations on the phonon spectrum, concluding with a brief summary.

II. MATERIAL AND METHODS

To obtain high-quality INS spectra, large single crystals of Cu-CPA were grown from solution. Starting with the synthesis method used to discover the material [12], we have optimized the growth process [24] to obtain crystals that extend up to linear sizes of 25 mm. These grow as platelets, with the other two dimensions spanning 2–4.5 mm and 0.5–2 mm; a typical crystal is shown in Appendix A. Microscopically, at low temperature (85 K) the compound realizes a monoclinic $P112_1$ space group with $a = 23.965$ Å, $b = 8.0765$ Å, $c = 18.282$ Å, and $\gamma = 90.35^\circ$. Because the material has a rather low density (2 g cm^{-3}) [12] and one Cu^{2+} ion provides the minimal spin of $S = 1/2$, it was necessary to coalign multiple crystals for our spectroscopic studies; two of these crystal assemblies are shown in Appendix A.

INS measurements were performed at a number of neutron sources. On the Continuous Angle Multiple Energy Analysis (CAMEA) multiplexing spectrometer at the PSI (Villigen, Switzerland) [25] we used an assembly of 12 deuterated single crystals with a total mass of 731.5(1) mg, coaligned to within 2.5°, and measured at two incident energies of 3.6 and 5.4 meV. These experiments allowed us to observe magnetic excitations and hence provided characterization information essential for our later studies, but the very large lattice constant of Cu-CPA (leading to the presence of many Bragg peaks on the detectors) caused significant spurious background scattering ("Currat-Axe spurions") arising when the INS angle happens to coincide with a Bragg reflection of the analyzer or the monochromator.

Time-of-flight experiments avoid this problem by not requiring crystals to analyze the energy transfer, and hence our subsequent high-resolution study was performed on the IN5 spectrometer [26] at the ILL (Grenoble, France), using a second batch of five large, deuterated single crystals with a total mass of 968.7(1) mg and coaligned within 1.0°. Because the two-leg ladders are aligned along the crystallographic b axis [Fig. 1(b)], both of these sample assemblies were oriented such that the b and c directions were in the scattering plane (and the a direction out of it). Additionally, we prepared a different sample consisting of seven deuterated single crystals with a total mass of 403.9(1) mg, coaligned to within 1.5°, and oriented with a and b in the scattering plane.

The incident neutron energies used to investigate the different excitation-energy ranges were 2.27 meV ($\lambda = 6$ Å), 2.70 meV ($\lambda = 5.5$ Å), and 5.11 meV ($\lambda = 4$ Å). To study the bottom of the magnetic excitation spectrum and the low-temperature acoustic phonon contribution, both at temperature $T = 0.05$ K, we used $E_i = 2.27$ meV to take advantage of the extremely fine energy resolution ($\Delta E \simeq 56$ μeV at the elastic line and smaller still at finite energy transfer); this fine resolution and the clean signal made it unnecessary to subtract any high-temperature scattering data representing the background. To investigate the complete magnetic spectrum and the temperature dependence of the phonon contribution, we used both $E_i = 2.70$ meV ($\Delta E \simeq 70$ μeV) and $E_i = 5.11$ meV ($\Delta E \simeq 170$ μeV), performing our measurements in a dilution refrigerator spanning the range 0.05–30 K. Measurements using a standard vanadium sample were performed for instrument calibration and background estimation. The quoted energy resolutions correspond to the full width at half-maximum (FWHM) height of the quasielastic line.

Finally, to investigate the effects of isotope substitution on the elastic properties, we performed an additional experiment on the LET spectrometer [27] at ISIS (Chilton, UK), using five large single crystals, four of which were undeuterated, with a net mass of 626.6(1) mg, and one deuterated with

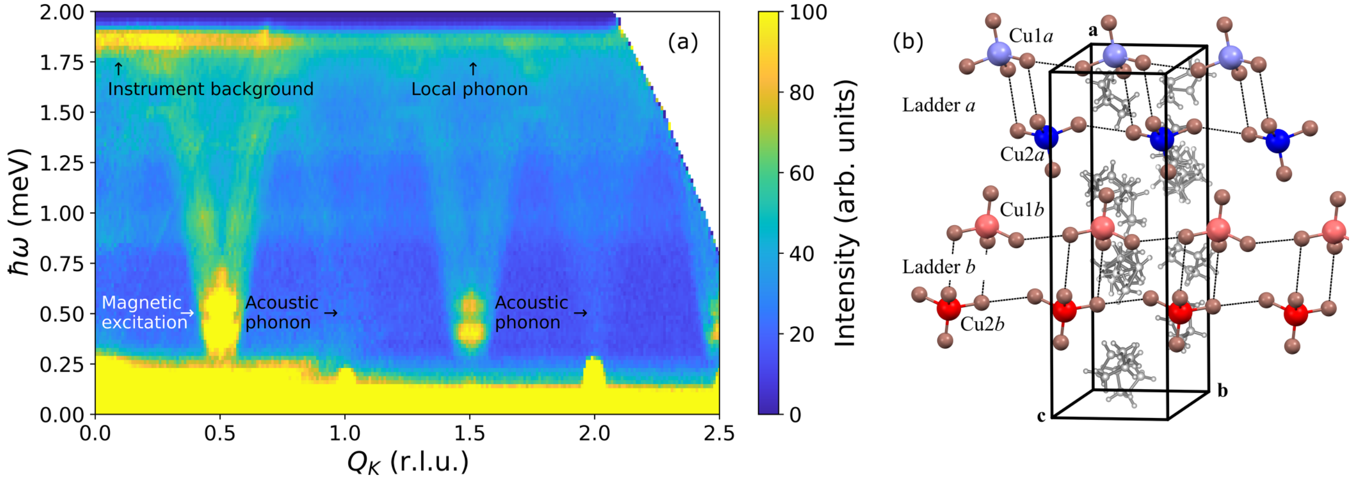

FIG. 1. Excitation spectrum and lattice structure of Cu-CPA. (a) Full excitation spectrum measured at $T = 0.05$ K on IN5, shown with no background subtraction. The measurements were performed with $E_i = 2.70$ meV and the data integrated perpendicular to the ladder direction over the ranges $Q_H \in [-0.85, 0.85]$ r.l.u. and $Q_L \in [-2, 4]$ r.l.u. The dispersive modes with high intensity at half-integer values of Q_K are the magnetic ("triplon") excitations of the $S = 1/2$ antiferromagnetic Heisenberg spin ladders. The dispersive modes appearing at integer values of Q_K are acoustic phonons, which have low intensity at this measurement temperature. Intensity contributions arising from low-lying local (optical) phonons and from the instrument background are also marked. (b) Low-temperature structure of Cu-CPA, showing the two inequivalent spin ladders (denoted as "Ladder *a*" and "Ladder *b*"). For clarity, only half of the crystallographic *c* direction is shown. Following the nomenclature introduced in the structural study of this material [24], the lighter and darker red and blue colors denote inequivalent Cu^{2+} ions on each ladder rung. Here we have shown the cyclopentylammonium (CPA) molecules in gray, projected behind the copper-tetrabromide units, in order to enhance the visibility of the ladders.

mass 14.5(1) mg. These crystals were coaligned within 1.0°, with the *b* and *c* directions defining the scattering plane. We took advantage of the energy-multiplexing capabilities of LET to measure simultaneously with the four incident neutron energies $E_i = 1.70$, 2.40, 3.70, and 6.40 meV. Due to their intrinsic energy scales, we resolved the magnetic excitations in our datasets taken with both $E_i = 2.40$ and 3.70 meV, while the phonons were best analyzed using $E_i = 3.70$ meV, where the energy resolution was $\Delta E \simeq 100$ μeV. Our CAMEA data were analyzed using the software package MJOLNIR [28] and our time-of-flight data using HORACE [29].

III. SPIN AND PHONON EXCITATION SPECTRA

We begin with the overview of the excitation spectrum shown in Fig. 1(a). It is evidently rather complex, with clear magnetic excitations, more than one type of phonon contribution on overlapping energy scales, and the usual instrumental backgrounds. One standard method for separating these contributions is through their Q dependence, because the spin excitations follow the magnetic form factor of Cu^{2+} whereas the phonons have a universal $|Q|^2$ form. In temperature, the phononic contributions can usually be isolated by measuring at higher thermal occupations, whereas the magnetic excitations in Cu-CPA lose coherence beyond 10 K and no magnetic contributions are discernible above 30 K. Nevertheless, a clear separation of the different components is made quite challenging in Cu-CPA by some unusually low optical phonon energies and an apparent "elastomagnetic" effect of the magnetic correlations on these phonons. To achieve the required separation, we analyze first its most straightforward contributions, which are the acoustic phonon branches and then the magnetic excitation branches in Fig. 1(a). After understanding these components, we characterize the unconventional phononic contribution with the aid of a reinterpretation of the measured specific heat.

A. Acoustic phonons

To isolate the acoustic phonon contribution to the spectrum, we investigate the excitation spectrum at high Q, which in Cu-CPA means around the point $\mathbf{Q} = (0\ 2\ 0)$, and at our highest temperature of $T = 30$ K, where no coherent magnetic excitations are present. A constant-energy scan at 1.6 meV, shown in Fig. 2(a), reveals a pair of concentric rings that are approximately circular, indicating the presence of two acoustic phonons. Full details of our data treatment are presented in Appendix B. By following the intensity profiles as functions of Q_K and Q_L, shown, respectively, in Figs. 2(c) and 2(d) for one selected energy-integration window, we reconstruct the dispersions of these two phonon branches to obtain the points shown in Fig. 2(e). In Fig. 2(b), where we have integrated over Q_L to show the intensity $I(Q_K, \omega)$, we notice that both phonon branches are visible, with the lower-lying branch corresponding well to the overplotted Q_L dispersion (blue diamonds). We remark here that both acoustic phonon branches seem to undergo an avoided crossing with the dispersionless modes providing the intense signal around 2 meV, and hence that one cannot expect follow these branches to their upper band edges.

We proceed by assuming the dispersion relation $\hbar\omega(k) = 2\hbar\sqrt{C/M}\sin(kd/2)$, where C is an effective spring constant, M an effective mass, and d the unit-cell dimension in the appropriate crystallographic direction. The speed of sound in the acoustic (small-k) regime is then directly proportional to the "reduced spring constant," $\sqrt{C/M}$, and also to the unit-cell

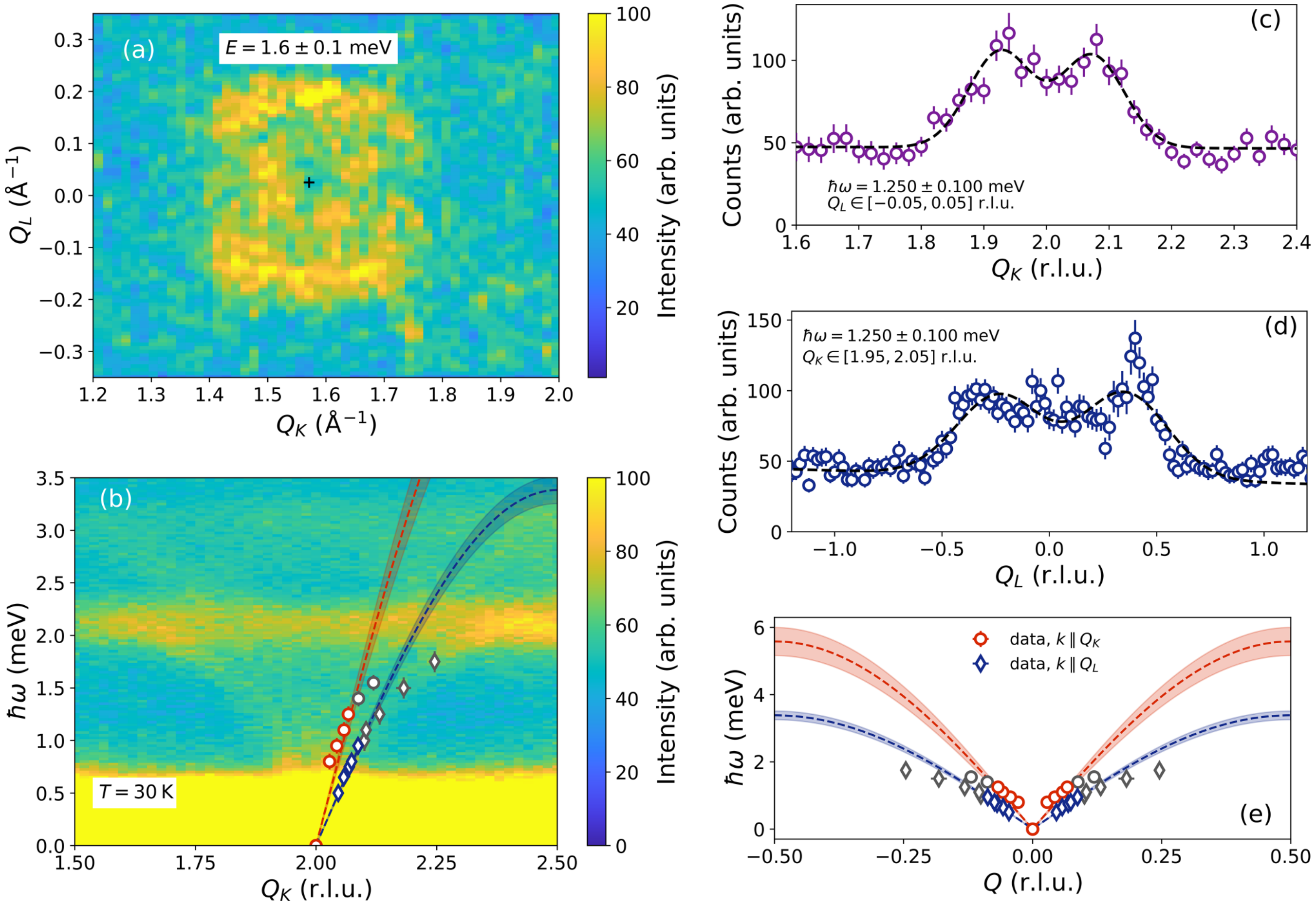

FIG. 2. Low-energy phonon dispersion of Cu-CPA, measured with $E_i = 5.11$ meV at $T = 30$ K. (a) Constant-energy slice integrated over the range (1.5, 1.7) meV to identify two rings in (Q_K, Q_L), around the point $\mathbf{Q} = (0\ 2\ 0)$, which are approximately circular in absolute units (Å^{-1}). (b) Intensity, $I(Q_K, \omega)$, obtained by integration over Q_H in the range $[-0.85, 0.85]$ r.l.u. and over $Q_L \in [-2, 4]$ r.l.u. to show the phonon contribution as a function of Q_K. Red circles represent phonon 2, which has stronger intensity along Q_K and is shown in (c); blue diamonds represent phonon 1, which has stronger intensity along Q_L and is shown in (d). (c), (d) Characteristic constant-energy slices prepared by integration over small energy and wave-vector intervals around $Q_L = 0$ and $Q_K = 2$, which yield the intensity profiles as functions of Q_K (c) and Q_L (d). (e) Deduction of two phonon dispersions from multiple constant-energy slices. Dashed lines represent the best fits to these phonons and shaded areas the σ fitting uncertainties. Gray symbols mark data points excluded from the velocity fit.

dimension, as we show in Appendix B. Approximating the speed of sound by measuring over a finite Q range around $Q = 0$, we obtain the two sound velocities $v_1 = 320(24)$ m s^{-1} for the softer mode (visible predominantly along Q_L) and $v_2 = 555(42)$ m s^{-1} for the stiffer one (visible along Q_K). Thus the velocities of sound in Cu-CPA are rather low, as expected for a soft organic compound. In Appendix B we quantify the four reduced spring constants obtained from these velocities, noting that our results show Cu-CPA to be structurally stiffer along the ladder (b) direction, which is a stack of inorganic (rung) units, than in the transverse direction, where the ladders are separated by large organic groups [Fig. 1(b)].

B. Magnetic excitations

The dynamical structure factor of the two-leg $S = 1/2$ spin ladder with pure-Heisenberg rung and leg interactions is dominated by a dispersive branch of $\Delta S_z = 1$ excitations. In the strong-rung limit, this branch is nearly flat at the energy $J_{\rm rung}$ of the singlet-triplet excitation on a single rung. As the leg-to-rung interaction ratio, α, is increased, it can be considered as a propagating triplet excitation dressed by quantum fluctuations of increasingly long range, which increase its band width, and this magnetic quasiparticle is known as the "triplon." The triplon is threefold degenerate at zero applied magnetic field and appears in the antisymmetric parity sector. As noted in Sec. I, the strong-rung regime ($\alpha \leqslant 0.5$), has been studied in detail in the context of BPCB and BPCC, and in the absence of an applied field is amenable to a number of analytical or expansion methods that yield the exact spectral shape and intensity. At higher α, however, only numerical techniques are able to compute the spectral function with quantitative accuracy, finding that the spectrum exhibits features combining those of the strong-dimer and strong-chain regimes. Among the candidate numerical methods, ED is limited in principle by the size of the system, which results in a discrete coverage of momentum space [30]. Systematic numerical expansion methods, despite a basis in the strong-rung limit, can access interaction ratios up to $\alpha \approx 3$ [31]. The density-matrix renormalization-group (DMRG) method

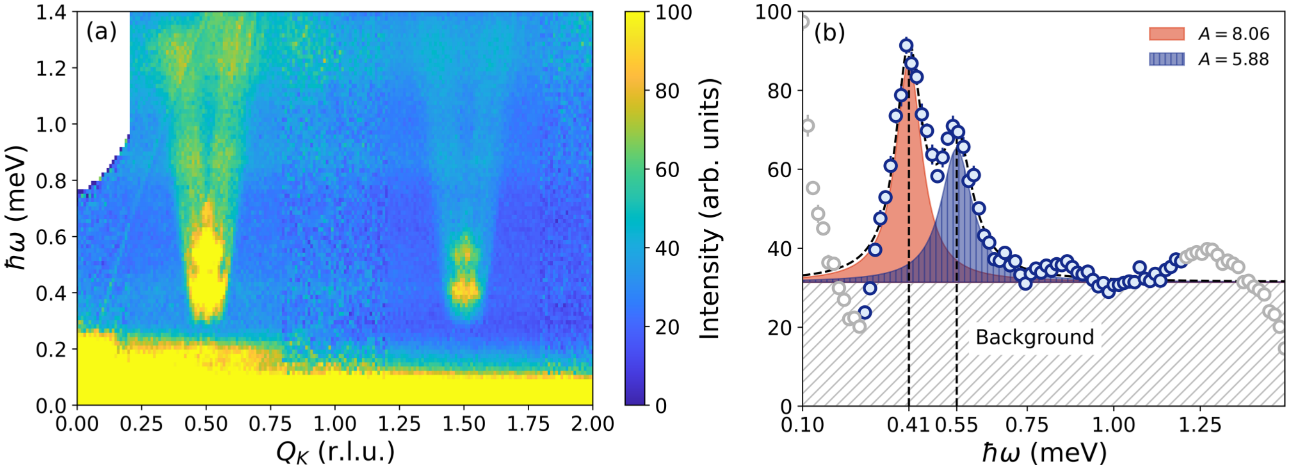

FIG. 3. Low-energy triplon dispersion of Cu-CPA, measured with $E_i = 2.27\,\text{meV}$ at $T = 0.05\,\text{K}$. (a) Intensity, $I(Q_K, \omega)$, obtained by integration over $Q_H \in [-0.85, 0.85]$ r.l.u. and over the full range of Q_L to reveal the two dispersive triplon branches. Bragg peaks and phonon contributions have been masked. (b) Constant-**Q** cut with $Q_K = 1.5$ r.l.u. and integration width $dQ_K = \pm 0.02$ r.l.u., integrating over the ranges $Q_H \in [-0.85, 0.85]$ r.l.u. and $Q_L \in [-2, 4]$ r.l.u. The two peaks were fitted with Lorentzians, whose center positions (dashed lines) were taken to estimate the two gaps and whose integrated intensities are shown in the legend. The fitting range (blue circles) was reduced to avoid the elastic line, the extension of its tail to $\hbar\omega \simeq 0.25\,\text{meV}$, and a dispersionless feature around 1.2 meV (data points not included in the fit are shown as gray circles). The hatched area represents a constant background contribution.

and its modern MPS reformulation are ideally suited for 1D systems and provide fully quantitative spectra for all energies and wave vectors at all α [4].

Although the magnetic component dominates the excitation spectrum at low temperatures and small Q values, as we showed in Fig. 1(a), a quantitative analysis requires a systematic subtraction of the phonon contribution. To deduce the phononic background to subtract from the spectrum measured at base temperature ($T = 50\,\text{mK}$), we treated our high-temperature dataset ($T = 30\,\text{K}$) by first masking the Bragg peaks and their tails, specifically from the elastic line up to a threshold energy of 0.2 meV. We then isolated the phonon contribution by considering only the second Brillouin zone, away from the spurious intensity contribution of the beam stop, and finally rescaled this intensity by the Bose function to account for the measurement temperature. The nonmagnetic background, therefore, contained a temperature-independent part (around the elastic line) and a temperature-dependent contribution most relevant at higher energy transfers.

We remark here that, in all our discussions of the magnetic excitations, we assume based on the structure of Cu-CPA that these are entirely 1D in nature and have integrated the INS intensities we analyze in both perpendicular momentum-transfer directions. We relegate to Appendix D the demonstration of this 1D character from our INS measurements.

1. Low-energy spectrum

We begin by addressing the low-energy part of the spectrum, which we measured at the extremely fine energetic resolution ($\Delta E \approx 56$ μeV) available on IN5 with $E_i = 2.27\,\text{meV}$. The low-energy spectrum is shown in Fig. 3(a), and as expected from the low-temperature crystal structure displays two distinct, gapped branches that disperse steeply from the half-integer Q_K points. The intensity $I(\hbar\omega)$ measured at $Q_K = 1.5$ r.l.u. is shown as the open circles in Fig. 3(b). We fitted the peaks with two Lorentzians above an assumed constant background, excluding the near-elastic contributions and nondispersive features beyond 1.2 meV by restricting the fitting range. This procedure yielded the fitting parameters shown in Table I. A key result is an accurate estimate of the two gaps as $\Delta_b = 0.41(1)\,\text{meV}$ and $\Delta_a = 0.55(1)\,\text{meV}$, a 34% difference corresponding well with the distortion parameter $\delta = 13.5\%$ estimated in Ref. [24]. Here we have assigned the smaller spin gap to Ladder b of Fig. 1(a) and the larger to Ladder a, basing this attribution on the observation of Ref. [24] that the largest difference between the two inequivalent ladders is in the Br-Br separations within the rung interaction pathways; the significantly shorter distance for Ladder a is likely to mean a stronger J_{rung} on this ladder and hence a larger gap. Because the mode linewidths, Γ_a and Γ_b, are much larger than the instrumental resolution, we conclude that they are intrinsic. The integrated intensities of the two peaks, shown by the red and blue shading in Fig. 3(b), obey the relation

$$r_{b/a} = \frac{S_b(Q)\hbar\omega_{\mathrm{Q},b}}{S_a(Q)\hbar\omega_{\mathrm{Q},a}} = \frac{8.06(60) \times 0.41(1)}{5.88(70) \times 0.55(1)} = 1.0(2), \qquad (1)$$

and hence reveal equal scattering contributions after correcting for the excitation energy.

TABLE I. Best-fit parameters for the two Lorentzian peaks shown in Fig. 3(b). The energy is taken from the peak center, Γ is the FWHM, and A is the integrated intensity.

Parameter	Ladder b	Ladder a
Energy gap (Δ, meV)	0.41(1)	0.55(1)
Linewidth (Γ, meV)	0.092(7)	0.110(14)
Intensity (A, arb. units)	8.06(60)	5.88(70)

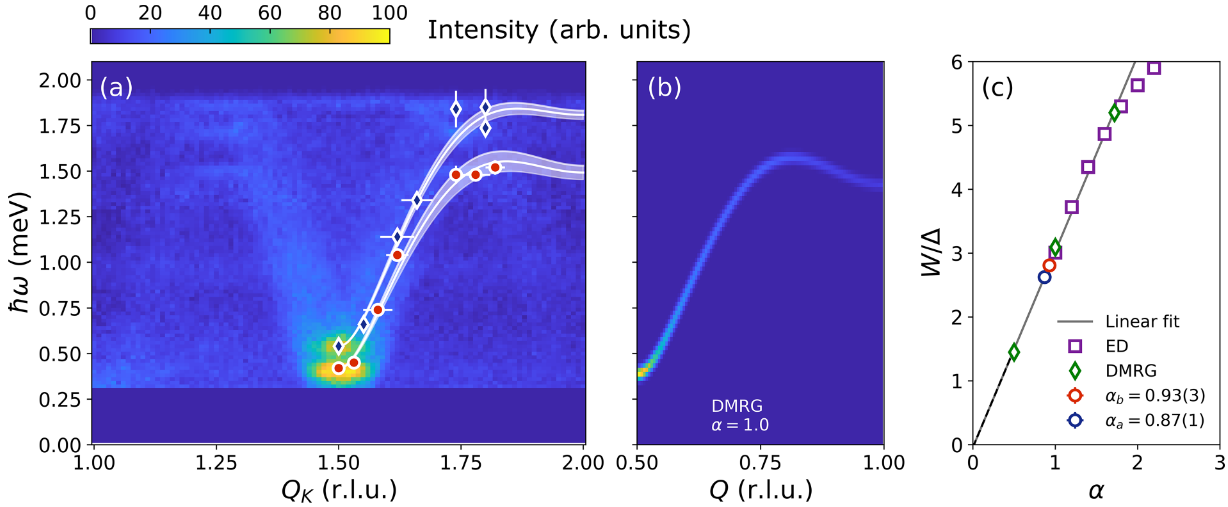

FIG. 4. Full magnetic excitation spectrum of Cu-CPA. (a) Double triplon dispersion determined by subtraction of the background and of the complete phonon contribution. The measurements were performed with $E_i = 2.70$ meV. We integrated the data over the ranges $Q_H \in [-0.85, 0.85]$ r.l.u. and $Q_L \in [-2, 4]$ r.l.u. Red circles (Ladder *b*) and blue diamonds (Ladder *a*) show the center positions of Lorentzian (Gaussian) fits to selected constant-**Q** (constant-energy) scans. Solid lines show best fits obtained by parametrizing the ladder dispersion relation as a function of α [32], as detailed in Appendix E. (b) Dynamical structure factor, $S(Q, \omega)$, calculated by density-matrix renormalization-group (DMRG) methods [4] for a two-leg ladder with leg-to-rung interaction ratio $\alpha = 1$ and with the energy scale selected to fit the gap Δ_b measured in experiment. (c) Bandwidth-to-gap ratio, W/Δ, of the ladder triplon, computed for a range of α values by ED and DMRG and compared with the results deduced for Ladders *a* and *b*. We draw attention to the remarkably wide regime of linear dependence (up to $\alpha = 1.6$) where $W/\Delta \approx 3\alpha$.

2. *Two-ladder dispersion*

Figure 4(a) shows the magnetic excitation spectrum of the two-ladder system measured with $E_i = 2.70$ meV at $T = 50$ mK. Qualitatively, we observe two dispersive branches with the gaps quoted in Table I at half-integer Q_K, which appear to remain distinct at all Q_K. They also appear to level off at band maxima around $\pi/2$ ($Q_K = 0.25$ r.l.u.), consistent with a drop in mode energy towards integer Q_K, although this is difficult to confirm because of the vanishing spectral intensity in this part of the Brillouin zone. In Fig. 4(b) we show that the shapes and intensities of both dispersive triplon branches, particularly that of Ladder *b*, are rather similar to that of the canonical $\alpha = 1$ ladder computed by DMRG in Ref. [4].

The highest energies we measured near the two upper band edges, 1.48(5) meV for the triplon branch of Ladder *b* and 1.85(10) meV for Ladder *a*, differ by approximately 25%, whereas the gaps differ by 34% (Sec. III B1), indicating that triplon *a* has a smaller bandwidth-to-gap ratio than triplon *b*. For completeness we remark that we see no evidence for a crossing of the two triplon dispersions, but nor can we exclude such a crossing only on the basis of Fig. 4(a). The mode intensities decrease with Q_K away from the gapped points until they vanish completely at the zone boundary; despite this handicap, we can attempt to estimate the Q_K position of the band maximum, the inflection point of the dispersion, and the bandwidth-to-gap ratio, thereby placing some constraints on viable α values for each triplon branch.

For a quantitative analysis, we perform ED calculations for a two-leg ladder with antiferromagnetic Heisenberg interactions J_{leg} and J_{rung} in the ratio α. In Fig. 4(c) we compare our results for the bandwidth-to-gap ratio as a function of α with those obtained by density-matrix renormalization-group (DMRG) calculations for different α values in Ref. [4]. It is clear that the bandwidth-to-gap ratio, which, in principle, is an experimental observable, constitutes an excellent measure of the α parameter of a ladder, with a monotonic dependence that is even linear over a remarkably broad range of α. Because the bandwidth is more sensitive to J_{leg} and the gap to J_{rung}, the monotonic dependence is no surprise, but the linearity up to $\alpha \approx 1.6$, where multiple nonlinear effects become apparent in any strong-coupling expansion, is surprising.

Because it is difficult to estimate the upper band edges accurately from our INS data [Fig. 4(a)], we proceed by applying the parametrization of Ref. [32] to the triplon dispersions computed by DMRG in Ref. [21]. Full details of the parametrization procedure are presented in Appendix E. By this approach we obtain a quantitative estimate of the interaction parameters of the two ladders as $J_{\mathrm{leg},b} = 0.74(3)$ meV and $J_{\mathrm{rung},b} = 0.80(4)$ meV $[\alpha_b = 0.93(3)]$ for the lower branch and $J_{\mathrm{leg},a} = 0.84(2)$ meV and $J_{\mathrm{rung},a} = 0.97(2)$ meV $[\alpha_a = 0.87(1)]$ for the upper. Thus we verify the deductions (above) that both ladders have α close to 1 and that $\alpha_a < \alpha_b$.

C. Spin-sensitive phonon modes

The final contribution to the spectrum that remains present after subtraction of the acoustic phonons [Fig. 2(a)] and the triplons [Fig. 4(a)] is a broad and nondispersive feature observed around 2.0 meV at $T = 30$ K [Fig. 2(c)]. In Appendix F we show that the powder average of this intensity is proportional to $|Q|^2$, verifying its phononic nature. Analysis of the integrated scattering intensity as a function of energy reveals that the flat band is composed of two distinct sets of

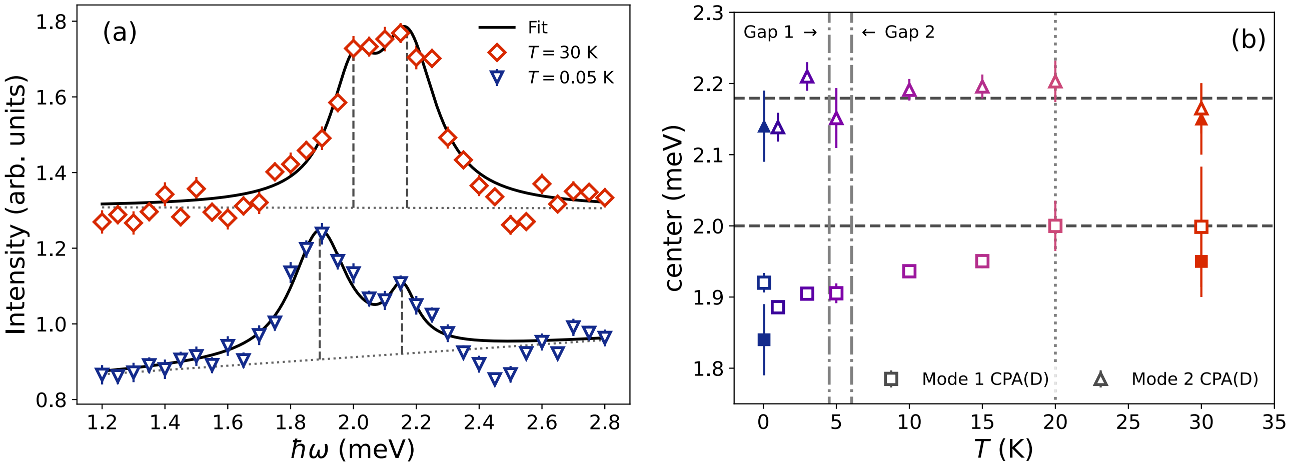

FIG. 5. Correlated elastic and magnetic effects. (a) Scattered intensity obtained by integration over the momentum ranges $Q_H \in [-0.85, 0.85]$ r.l.u., $Q_K \in [1.88, 1.92]$ r.l.u., and $Q_L \in [-2, 4]$ r.l.u., shown as a function of energy transfer at our highest and lowest temperatures to characterize the evolution of the two distinct types of low-lying vibrational mode associated with the CPA molecules. The lower modes shift to lower energies upon cooling, whereas the upper modes remain at a constant energy but appear to lose intensity to lower energies. (b) Temperature-dependence of the center positions of the two mode types (triangles and squares) required to fit the scattered intensity, obtained from Lorentzian profiles. The dashed lines serve as guides to the eye. Most error bars are smaller than the symbol sizes. The downward shift in the lower mode energies (squares) below 20 K suggests an association with the onset of magnetic correlations.

modes, seen in Fig. 5(a), whose positions and weights change significantly between $T = 30$ and $T = 0.05$ K.

1. *Putative elastomagnetic effect*

Analyzing this thermal evolution in detail, in Fig. 5(b) we observe that the upper set of modes is temperature independent, centered at $\hbar\omega = 2.17(3)$ meV, whereas the energy of the lower set is reduced upon cooling, from $\hbar\omega = 2.00(2)$ meV at 30 K to 1.90(2) meV at base temperature. More specifically, the frequency shift of the lower modes shows a rather abrupt onset below 20 K, then develops continuously down to 6 K, below which it saturates. The fact that 20 K coincides with the emergence of magnetic correlations and 6 K is the gap temperature forms an important piece of evidence suggesting that the origin of the phonon frequency shift lies in the spin sector, i.e., in an elastomagnetic effect.

First we remark that phonon frequencies do change with temperature alone, conventionally hardening, or less often softening, monotonically from some hundreds of Kelvin and saturating on approach to zero. In an organic framework material such as Cu-CPA, we cannot exclude that phonon-phonon interactions could become apparent only below the mode energy of 20 K, which would act to shift and split the manifold of low-energy phonons. However, two further features of Fig. 5(b) are consistent with an elastomagnetic effect and difficult to reconcile with a purely phononic one. One of these is the fact that phonon-phonon interactions alone should preserve the average energy of the manifold of modes, whereas the net downward shift we observe in Fig. 5(a) implies the involvement of a second sector in addition to the lattice sector (which from the characteristic temperatures we would assume to be the magnetic sector). The other is the fact that only half of the phonon modes show this behavior, apparently allowing us to benchmark an elastomagnetic frequency shift against conventional thermal evolution at the lowest temperatures. Nevertheless, because our measurements are already at the limits of sensitivity, challenging our ability to perform a reliable separation of magnetic contributions from both conventional and local phononic contributions, we cannot exclude the possibility that our attribution of local-phonon contributions does miss the higher-lying modes that would preserve the average energy, and hence we refer to our elastomagnetic effect as "putative."

To seek independent evidence for or against an elastomagnetic effect, we draw attention to the fact that the temperature of the change in stiffness of the lower dispersionless phonon modes correlates closely with changes in the magnetic susceptibility that occur as correlations set in. The lower local phonons undergo a 5% softening as a result [Fig. 5(b)], which is a very large relative change when compared with the 0.5% effect observed in the compound $(C_4H_{12}N_2)Cu_2Cl_6$ [33] and the 1% effect found in $SrCu_2(BO_3)_2$ under pressure [34]. To understand the origin of such a "giant" elastomagnetic softening, and to connect directly with the fact that only half of the local phonon modes show it, we observe that the four inequivalent CPA molecules in Cu-CPA form two groups, one pair lying far from the Cu ladders and the other pair having their ammonium group lying very close to the ladder rungs, as shown in Fig. 6(a).

To gauge the distances between the ammonium groups and the Br atoms lying directly on the two Cu-Br-Br-Cu superexchange pathways making up each rung, we define a plane formed by these four Br atoms, shown by the shaded surface in Fig. 6(b), which is crudely a rhombus with an 80° interior angle and side lengths of 3.6 Å (adjoining one Cu atom) and 4.4 or 4.5 Å (across the rung). In both NH_3 groups of a single rung unit, one of the H atoms is far (3.7 Å) from this plane and one is located at $d_2 \simeq 3.3$ Åfrom it, but the third H atom is only $d_1 = 2.3$ Åaway. The distance of this atom from the nearest Br atom is only $d_0 = 2.61$ Å[Fig. 6(b)], which is short compared to the Br-Br spacings. Taking this H

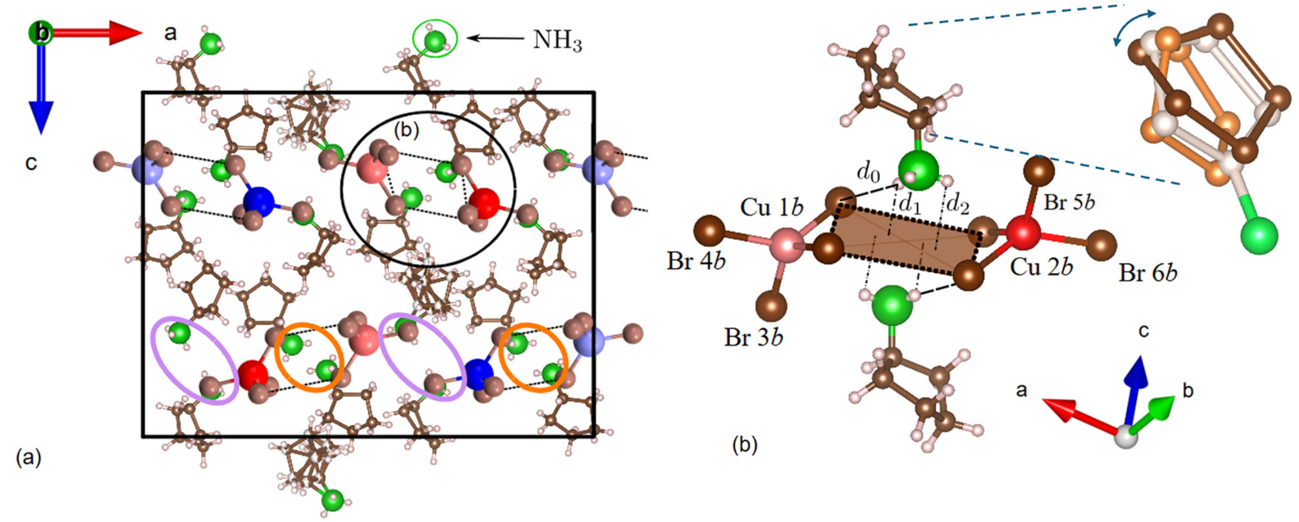

FIG. 6. Involvement of CPA molecules in ladder magnetism. (a) Low-temperature crystal structure of Cu-CPA, showing four ladder rungs that each contain a pair of NH_3 groups from a CPA molecule within the rung-superexchange volume; two of these pairs are circled in orange. In contrast, the NH_3 groups of the remaining two CPA molecules per ladder are situated well outside the rungs; two of these pairs are circled in purple. The black circle denotes one rung unit that is displayed in a different projection in (b). (b) Visualization of the rung superexchange volume based on the nearly square trapezium formed by the four Br atoms involved in the two Cu-Br-Br-Cu paths. The proximity of individual H atoms of the ammonium group to the nearest Br atom (d_0) and to the rung plane (d_1 and d_2) suggests the involvement of ammonium electrons in virtual hopping processes between the halogen atoms, and hence in the rung spin interaction. Inset: representation of the two conformations (brown, orange) of the cyclopentane ring C16-C20 measured above the order-disorder transition [24], suggesting the nature of the local phonon modes (double-headed arrow); white atoms represent the low-temperature conformation of this ring.

atom to measure the extent of the relevant lone-pair orbital of the strongly electronegative N atom, it is clear that this does lie close enough to affect the electronic correlations on the rung, and hence that the ammonium group can be considered as part of one pathway for virtual hopping processes contributing to the rung magnetic correlations. This establishes a clear causal connection between the spin sector and the lattice dynamics of half of the local phonon modes.

2. *Identification of local phonon modes*

The final task in understanding the putative elastomagnetic effect is to identify the nature of the local phonon modes. A natural assumption based on the observations of the previous paragraph would be that they involve the NH_3 groups [Fig. 6(b)]. In general one expects that vibrational modes of light atoms such as N and H would lie at energies very much higher than 2 meV. By contrast, rotational modes are conventionally found at GHz frequencies, and a neutron scattering study of ammonium rotations in NH_4Br reported these to be in the quasielastic regime (below 0.5 meV) [35]. We did find one report of NH_3 librations at 2.7 meV in a very weakly bonded system [36].

For deeper insight into the nature of these modes, we exploited the fact that we had both hydrogenated and deuterated samples to search for an isotope effect. Here we stress that the low-temperature phonon frequency shift is isotope independent, and in Fig. 5(b) we used our data from deuterated Cu-CPA because these had better statistics. In Appendix F we show that the average energy of the local phonons, meaning the average over the two peaks in Fig. 5(a), shows a clear H-D isotope effect, with the two energies differing by 6(1)%. Taking the vibrational energy to obey a simple proportionality to $1/\sqrt{m}$, where m denotes the mass of a molecule, this result is consistent only with the partial (at least 75%) or complete deuteration of an entire CPA molecule [Appendix F]. Most importantly, it seems to exclude the possibility that the mode could be a rotation of the NH_3 groups, where (with the N atoms fixed) one would anticipate frequencies in the ratios $\sqrt{4/3}$, $\sqrt{5/3}$, or $\sqrt{6/3}$, and points instead to a mode of the cyclopentane ring.

To understand the nature of a low-energy mode of the ammonium-bonded C_5H_9 ring, we appeal to our interpretation of the order-disorder transition that we found in Cu-CPA at $T^* = 136\,\mathrm{K}$ (132 K when deuterated). In Ref. [24] we showed that one of the four cyclopentane rings has two possible conformations at $T > T^*$, and these are superposed on each other in the inset of Fig. 6(b). This provides a plausibility argument for low-lying modes related to the switching of the cyclopentane rings from one conformation into the other: the predominantly out-of-plane atomic displacements involved are subject to much lower restoring forces than in-plane displacements, and the relative distortion of the ring (perhaps best characterized as a folding about one of several possible in-plane axes) seems to be weak. We note further the possibility that these modes are particularly low-lying due to the evident proximity of the system to the order-disorder transition.

In summary, the body of evidence indicates that, as magnetic correlations become established with decreasing temperature, the electronic orbitals of the H and N atoms undergo nontrivial alterations that affect the low-energy elastic properties of the entire CPA molecule, causing its characteristic local phonon modes to undergo a change in frequency.

While this logic provides no value for such a frequency shift, beyond the expectation that it should be "weak," our experimental measurement of a "giant" 5% shift sets a clear target for electronic structure calculations to confirm or deny. Although a purely phononic effect may be a more natural candidate for 5% frequency shifts, explaining the phenomenology of Cu-CPA in this way would seem to require some coincidences (in temperatures scales) and accidents (in missing intensity) that currently make the elastomagnetic scenario more plausible.

IV. ELASTIC AND MAGNETIC CONTRIBUTIONS TO THE LOW-TEMPERATURE SPECIFIC HEAT

In Sec. III we determined the definitive magnetic interaction parameters of Cu-CPA and discovered two sets of local (nondispersive) phonon modes of the CPA molecules that are centered around 2.0 meV at low temperatures. Both results point towards the need to revisit the interpretation of the specific-heat data presented in Ref. [24]. First, our determination of the four J parameters leads necessarily to an unambiguous calculation of the magnetic contribution. Second, modeling the phonon contribution with the Debye formula, using a Debye temperature $T_{\mathrm{D}} = 173(4)\,\mathrm{K}$ chosen to fit the high-temperature specific heat ($40 \leqslant T \leqslant 80\,\mathrm{K}$), makes this contribution vanishingly small at low temperatures, and in no way reflective of multiple low-lying local vibrational modes. To compensate for this lack of low-energy phonon contributions, the previous best fit to a two-ladder model found the gaps $\Delta_1 = 0.32(2)\,\mathrm{meV}$ and $\Delta_2 = 0.42(2)\,\mathrm{meV}$, which our INS measurements demonstrate to be artificially small.

To reconcile our specific-heat and spectroscopic measurements, we introduce a contribution from low-lying and dispersionless phonons that we assume can be modeled as harmonic oscillators (Einstein phonons) with an Einstein temperature $\Theta_{\mathrm{E}} \simeq 20\,\mathrm{K}$ (corresponding to the mode centers). For the magnetic specific heat, we extend the model of Ref. [37] to the two-ladder system by fixing the two gap values to $\Delta_b = 0.41(1)\,\mathrm{meV}$ and $\Delta_a = 0.55(1)\,\mathrm{meV}$, and the two magnon velocities, calculated in detail in Appendix C, to $c_b = 234(10)\,\mathrm{m\,s^{-1}}$ and $c_a = 268(10)\,\mathrm{m\,s^{-1}}$. We also retained a Debye model to account for the high-temperature phonon contributions. By a recursive fitting of the Einstein and Debye models, in which we performed successive relaxations of the Einstein temperature and the weight factor C_{E} of the local-phonon contribution, and then of the Debye temperature and weight factor, we obtained the values $\Theta_{\mathrm{E}} = 17.9(3)\,\mathrm{K}$, $C_{\mathrm{E}} = 8.1(3)\ \mathrm{J\,s^{-1}K^{-1}mol^{-1}}$, $T_{\mathrm{D}} = 178.1(44)\,\mathrm{K}$, and $C_{\mathrm{D}} = 82(2)\ \mathrm{J\,s^{-1}K^{-1}mol^{-1}}$.

The fit to the data reported in Ref. [24] is shown in Fig. 7 and a fit over the full temperature range can be found in Appendix G. First we remark that local phonons at $\Theta_{\mathrm{E}} = 17.9\,\mathrm{K}$, combined with the true gaps of the triplon contribution, provide a quantitatively accurate fit to the low-temperature specific heat. The weight of the local phonon modes is approximately 10% of the total phonon contribution, which is an eminently reasonable value. The small deviation of the measured phononic contribution, $C_{\mathrm{ph}}(T)$, from the model over the range from 1–2 K remains as an experimental challenge. The overall fit also shows a weakness in the range 20–30 K, which could possibly be improved by adding another local phonon with $\Theta_{\mathrm{E}} \simeq 40\,\mathrm{K}$, but in the absence of spectroscopic confirmation we do not follow this empirical route. In summary, our quantitative understanding of the low-energy magnetic and phononic excitations (Sec. III) leads us to an accurate determination of the specific heat, thereby unifying spectroscopy and thermodynamics.

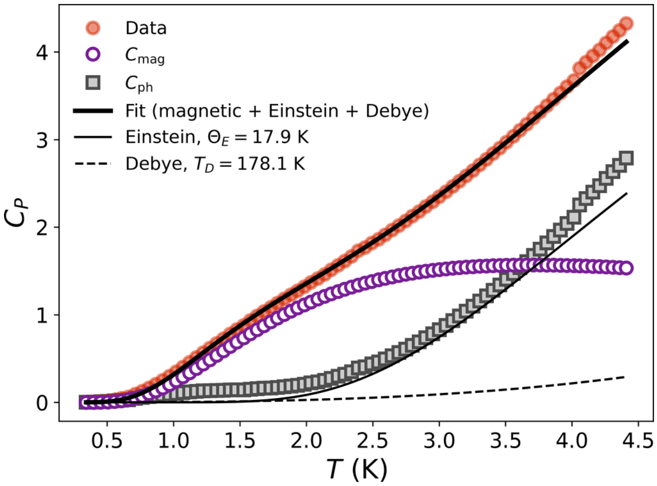

FIG. 7. Low-temperature specific heat. Three-component fit to the measured specific heat [24] using the precisely determined magnetic interactions, a Debye model for the phononic contribution at high temperatures, and an additional Einstein oscillator to account for the low-lying local phonon mode found by spectroscopy.

V. DISCUSSION

By measuring the dynamical spectral function we have established that Cu-CPA possesses unusually many and low-lying optical phonon excitations. The number of phonon modes can be traced to the presence of many CPA rings per unit cell of this metal-organic material, and their nature is already suggested by the fact that an order-disorder transition between distinct CPA ring conformations was discovered at a temperature $T^* = 136\,\mathrm{K}$ ($T^* = 132\,\mathrm{K}$ in the deuterated system) [24]. As to their anomalously low-lying nature, in Ref. [24] we also discovered an orthorhombic-to-monoclinic structural phase transition at $T^{\mathrm{mono}} = 113\,\mathrm{K}$ ($T^{\mathrm{mono}} = 119\,\mathrm{K}$ when deuterated), which suggests the presence of nearly soft phonons, potentially of several different types, in proximity to the transition. The low energies of the CPA phonons provide an additional reason for their sensitivity to the development of strong magnetic correlations on the double Cu-Br-Br-Cu superexchange paths of the ladder rungs, within which lie two ammonium groups of separate CPA molecules. A microscopic mechanism for this effect would be a target for cluster calculations addressing the spin-polarized electronic densities with and without magnetic correlations. This would then inform a discussion of the elastic properties of CPA with and without "magnetically pinned" ammonium.

Turning to the magnetic excitations, we have established the presence of two conventional triplon branches whose dispersions reflect two ladders with leg-to-rung coupling ratios of $\alpha \approx 1$. We comment that the improved understanding of Cu-CPA which we have developed over the course of our studies has involved a significant downward estimation of α, from values of order 2 based on early susceptibility measurements [12] to a much larger gap (smaller α) from specific-heat measurements [24] to a still smaller α using spectroscopic information. This evolution replicates the trajectory followed by DIMPY [19,37,38], underlining the difficulties inherent to estimating magnetic interaction parameters on the basis of thermodynamic measurements alone. In Cu-CPA we have not been able to find any evidence for sizable interactions between the two inequivalent ladders, which would be one route to nontrivial triplon mixing phenomena in a two-ladder system.

Having identified both the low-energy phonons and the triplons, we have been able to provide an accurate interpretation of the low-temperature specific heat measured in Ref. [24]. The sizes of the different contributions from these modes to any thermodynamic quantity remain difficult to deduce from spectroscopy, and the measurements show that approximately 10% of the phononic contribution in Cu-CPA lies in optical phonons around 20 K (2 meV). One way to discern whether or not further local phonons are present in the spectrum beyond the range of our INS measurements would be to subtract the magnetic and Debye (high-temperature phononic) contributions from the measured specific heat, which might reveal a local-phonon signal that contains further characteristic energies above 2 meV.

The fact that Cu-CPA contains phonon modes whose energy is very sensitive to spin correlations makes it a prime candidate for the study of hybridized spin and lattice dynamics. Taking the term magnetoelastic to cover changes in magnetic properties due to lattice effects, we have named the converse type of behavior we deduce (changes in elastic properties due to intrinsic dynamic magnetic effects) “elastomagnetic,” where we remark that neither magnetic order nor an applied magnetic field is required to change the elastic response. Clearly a soft material such as Cu-CPA is a suitable candidate for accurate measurements of magnetoeleastic behavior using both hydrostatic and uniaxial applied pressures. Dynamical spin-lattice hybridization phenomena induced by using coherent THz light to drive selected phonon modes have been given the name “magnetophononics” [39–41]. Although Cu-CPA can be expected to exhibit magnetophononic behavior, the very low excitation energy scales and the complexity of the phonon spectrum would pose a challenge to quantitative interpretation.

To summarize, we have measured the dynamical structure factor of a previously unexplored two-ladder quantum spin system. Beyond our definitive determination of the magnetic interaction parameters of the two inequivalent ladders, we have observed low-energy spectral weight reflecting the presence of unusually low-lying and local optical phonon excitations. In addition to the expected sensitivity of the magnetic Hamiltonian to static lattice effects, we establish the sensitivity of half of the low-energy local phonons to dynamical spin correlations, in the form of appreciable shifts in the phonon energy that coincide with the establishment of magnetic effects at low temperatures. These results position Cu-CPA as a candidate elastomagnetic system for future studies both by static lattice control using applied pressure and by dynamical lattice control in ultrafast nonequilibrium settings.

ACKNOWLEDGMENTS

We thank N. Casati, D. Fabini, S. Galeski, C. Kollath, B. Lake, K. Povarov, A. Razpopov, and R. Valentí for helpful discussions. J.P. acknowledges the financial support of the Universität Zürich through a UZH Candoc Grant. This project was supported by the Horizon 2020 research and innovation program of the European Union under the Marie Skłodowska-Curie Grant (Agreement No. 884104, PSI-FELLOW-III-3i). We acknowledge funding from the Chalmers X-ray and Neutron Initiative and support by the Wallenberg foundation though Grant No. 2021.0150. We are grateful to the Paul Scherrer Institute for the allocation of neutron beam-time on CAMEA at SINQ (under Project No. 20212923). Experiments at the ISIS Neutron and Muon Source were supported by beamtime allocation RB2210245 from the Science and Technology Facilities Council. Y.S acknowledges funding from the Swedish Research Council (Dnr. 2025-08127). M.M. acknowledges funding from the Swedish Research Council, VR (Dnr. 2021-06157 and Dnr. 2022-03936), the Swedish Foundation for Strategic Research (SSF) within the Swedish national graduate school in neutron scattering (SwedNess), and the Carl Tryggers Foundation for Scientific Research (CTS-222374).

DATA AVAILABILITY

The data that support the findings of this article are openly available [42–44].

APPENDIX A: SINGLE CRYSTALS AND INS SAMPLES

Figure 8(a) shows a photograph of one deuterated single crystal of Cu-CPA, as obtained from our optimized growth procedure. Figures 8(b) and 8(c) show two different assemblies of these crystals with different scattering planes, both of which were used for our neutron spectroscopy measurements at IN5.

APPENDIX B: ACOUSTIC PHONON VELOCITIES

Figure 1 shows that the acoustic phonons overlap with the energy scale of the magnetic excitations and that the top of the triplon bands coincides in energy with a local phonon contribution. Extracting the magnetic excitations therefore requires a comprehensive understanding of the phononic contribution to the spectral function of Cu-CPA, and for this it is most convenient to work around $\mathbf{Q} = (0, 2, 0)$, where the phononic part is most intense. We reiterate that the full phonon spectrum is inordinately complicated due to the fact that there are 328 atoms in the unit cell of the low-temperature structure of Cu-CPA [24]. However, our previous measurements of the magnetic specific heat and susceptibility [24], combined with the temperature-dependence of the magnetic excitations observed here, demonstrate that all magnetic contributions are negligible at 30 K. Thus we characterize the phononic contribution at this temperature.

Working in the (Q_K, Q_L) scattering plane [Fig. 2(a)], we integrated the measured intensities over a finite energy-transfer window, $\hbar(\omega \pm \delta\omega)$, and over a narrow strip around

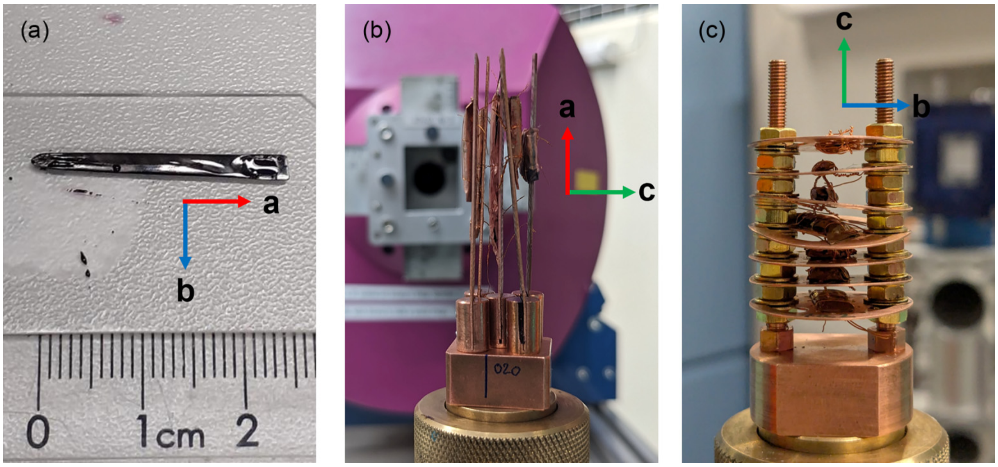

FIG. 8. Samples. Images of (a) a single crystal of deuterated Cu-CPA, (b) an assembly of five deuterated single crystals used in the IN5 experiment with *bc* as the scattering plane, and (c) an assembly of seven single crystals used in the IN5 experiments with *ab* as the scattering plane.

one of the in-plane momenta, i.e., $\mathbf{Q} = (0, 2 \pm 0.05, Q_L)$ and $\mathbf{Q} = (0, Q_K, \pm 0.05)$, to resolve the two phonons appearing around $\mathbf{Q} = (0, 2, 0)$. All of these Q_K or Q_L cuts were prepared by integrating in the direction parallel to the detector (Q_H) over the range $[-0.85, 0.85]$ r.l.u. and the perpendicular direction over a smaller range (typically 0.1 r.l.u.). The energy-integration range, $\delta\omega$, was determined from the energy resolution (defined by the FWHM of the elastic line), which depended on the neutron wavelength. The resulting intensities, $I(Q, \omega)$, were then fitted using two Gaussians on top of a linear background, as shown in Figs. 2(c) and 2(d), and the acoustic phonon dispersions gathered in Fig. 2(e).

Using the acoustic phonon dispersion relation

$$\omega(k) = 2\sqrt{\frac{C}{M}}\left|\sin\left(\frac{1}{2}kd\right)\right| \tag{B1}$$

in the long-wavelength (small-k) limit yields the phonon velocity

$$v = d\frac{\pi}{\hbar}\sqrt{\frac{C}{M}}. \tag{B2}$$

As noted in Sec. III A, we found only two different sound velocities due to the approximate fourfold symmetry of the phonon dispersion shown in Fig. 2(a), and measured these as $v_1 = 320(24)$ m s^{-1} and $v_2 \simeq 555(42)$ m s^{-1}. Dividing by the lattice dimension and the other constants leads to the four reduced spring constants $\sqrt{C_{1b}/M} \simeq 1.64(13)$ meV, $\sqrt{C_{2b}/M} \simeq 2.84(22)$ meV, $\sqrt{C_{1c}/M} \simeq 0.725(55)$ meV, and $\sqrt{C_{2c}/M} \simeq 1.25(10)$ meV. The higher stiffness along the crystallographic b direction is consistent with the general understanding of the crystal structure [Fig. 1(b)], where the two pairs of inequivalent spin ladders are aligned along b and separated along the a and c directions by the large CPA molecules.

APPENDIX C: TRIPLON VELOCITY

The effective velocity of a gapped triplon branch is obtained from a parabolic approximation to the low-energy part of its dispersion [45,46],

$$\hbar\omega_q \simeq \sqrt{\Delta^2 + c^2|q_\parallel - \pi|^2}, \tag{C1}$$

where Δ is the spin gap and $q_\parallel = 2\pi Q_K$. The velocity is then obtained as [47]

$$c = \left.\frac{\mathrm{d}\sqrt{(\hbar\omega_q)^2 - \Delta^2}}{\mathrm{d}(2\pi Q_K)}\right|_{Q_K=0.5}, \tag{C2}$$

where we computed the derivative as a divided difference, working over a relatively small range of Q_K (0.06 r.l.u.) and with a very small step size of $\Delta Q_K \simeq 0.01$ r.l.u. In this way we obtained the two triplon velocities as $c_b = 0.191(8)$ meV (r.l.u.)$^{-1}$ ($\equiv 234(10)$ m s^{-1}) and $c_a = 0.218(8)$ meV (r.l.u.)$^{-1}$ ($\equiv 268(10)$ m s^{-1}).

APPENDIX D: 1D NATURE OF MAGNETIC EXCITATIONS

We present INS data demonstrating that the magnetic excitations (triplons) of the two inequivalent ladders are entirely 1D in character. For this we show in Fig. 9 scattered intensities measured in reciprocal-space directions perpendicular to the ladder dispersion (Q_K). In Fig. 9(a) we integrate over an energy range covering the gaps of both triplons, $E = [0.3, 0.7]$ meV, as well as a relatively large portion of the detector coverage in Q_H ($Q_H = [-0.75, 0.75]$ r.l.u.). This dataset was prepared using equidistant Q-steps of size 0.02 Å^{-1}, which correspond to $dQ_K = 0.025$ r.l.u. and $dQ_L = 0.056$ r.l.u. The intensities of the two clear stripes at $Q_K = 0.5$ and 1.5 follow the magnetic form factor of Cu^{2+}. In Fig. 9(b) we demonstrate the absence of triplon dispersion in Q_H (prepared using steps of 0.075 r.l.u.) and in Fig. 9(c) the absence of dispersion in Q_L (with steps of 0.056 r.l.u.); the width of the energy bins in both panels is $\delta\hbar\omega = 15$ μeV, which corresponds to the energy resolution, and in both we integrated over $Q_K = [1.45, 1.55]$ r.l.u.

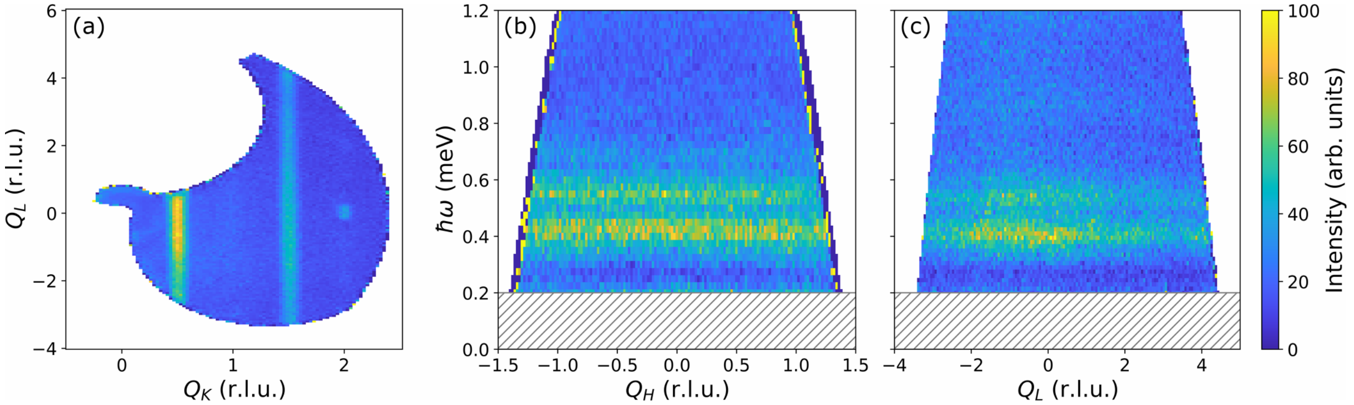

FIG. 9. One-dimensional magnetic behavior of Cu-CPA. (a) Intensity contour map in (Q_K, Q_L), with integration over the energy range $E = 0.4 \pm 0.1$ meV. (b) Intensity contour map in (Q_H, E), with integration over $Q_K = 1.50 \pm 0.05$ r.l.u. and $Q_L = 0.0 \pm 1$ r.l.u. (c) Intensity contour map in (Q_L, E), with integration over $Q_K = 1.50 \pm 0.05$ r.l.u. and $Q_H = 0.0 \pm 0.85$ r.l.u. The high-intensity bands shown in all three panels represent the gap(s) of the magnetic excitations.

APPENDIX E: PARAMETRIZED SINGLE-MODE APPROXIMATION

The single-mode approximation (SMA) is a very robust, if heuristic, approach to fitting the primary features of a spectral function. Introduced in the context of spin ladders in Ref. [32], it has since been used widely for the analysis of triplon dispersion relations [19]. The dispersion is expressed in the form

$$\hbar\omega(k) = \sqrt{\Delta^2 \sin^2\left(\tfrac{1}{2}k\right) + A^2 \cos^2\left(\tfrac{1}{2}k\right) + B^2 \sin^2(k)}, \quad \text{(E1)}$$

with the parameters Δ for the energy gap, A for the energy at the zone boundary $[\hbar\omega(k = 0)]$, and B capturing the leading nontrivial contributions. To extract the α values for the two inequivalent spin ladders in Cu-CPA, we applied the SMA to the DMRG calculations shown in Fig. 6 of Ref. [4] in order to obtain unbiased estimates of the three fit parameters Δ, A, and B over a range of α from 0.5 to 5. Based on these values, which are shown as the solid squares in Fig. 10 and reported for completeness in Table II, we implemented a cubic spline interpolation, shown as the solid lines in Fig. 10, that allows us to reproduce the triplon dispersion over a continuous range of α.

To verify this parametrization, we performed ED calculations and fitted the dominant branch of the resulting spectra with the SMA to extract a further set of Δ, A, and B parameters, which are shown as the open circles in Fig. 10. We find good agreement with the cubic spline interpolations, with minor quantitative deviations reaching the 10% level on Δ and A (5% on B) at larger α, where the short ladder lengths treated by ED become more of a handicap. For this reason we relied on DMRG at larger α, where multiple measurements on DIMPY ($\alpha = 1.72$) have established quantitative accuracy [19,21,48]. At small α, we compare our interpolation with results from the strong-rung regime by using Eq. (8) of Ref. [49] to obtain the Δ, A, and B parameters shown as open diamonds in Fig. 10. As expected, the strong-rung approximation (applied in Ref. [49] as an expansion to third order in α) is quantitatively accurate in the range $\alpha < 0.5$, but shows appreciable deviations beyond this that result in qualitative changes to the shape of the triplon dispersion.

We mention here that the numerical calculations (DMRG and ED) treat the magnetic excitation in units of J_{leg}. Thus in our parametrization procedure we do not fit $\hbar\omega$, but rather

TABLE II. SMA parameters extracted from the DMRG calculations of Ref. [4]. These parameters are shown as the squares in Fig. 10 and were used to calculate the cubic spline interpolation shown as the solid lines in Fig. 10.

α	Δ/J_{leg}	A/J_{leg}	B/J_{leg}
0.50	1.278(9)	3.128(8)	0.898(25)
1.00	0.495(8)	1.890(8)	1.355(9)
1.72	0.230(12)	1.130(8)	1.543(7)
5.00	0.068(21)	0.379(10)	1.619(5)

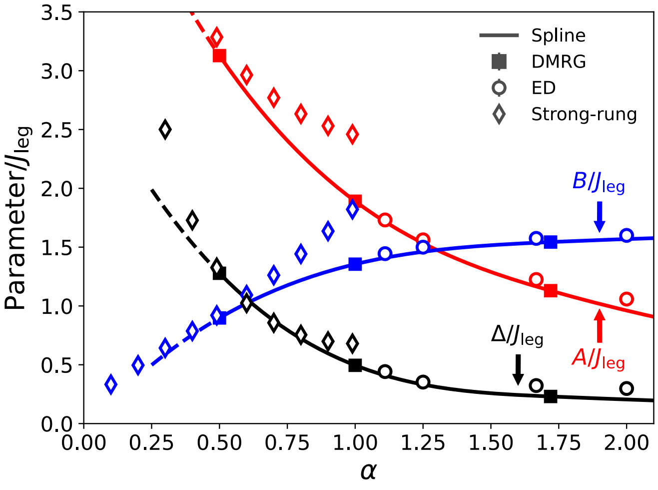

FIG. 10. Parametrization of the triplon dispersion in the single-mode approximation (SMA). Dependence on α of the three SMA parameters Δ (black), A (red), and B (blue). We parametrized the SMA as a function of α by a cubic spline interpolation based on the DMRG calculations of Ref. [4], which are shown as solid squares. The SMA parameters derived from our ED calculations are shown as the open circles and the parameters obtained within the strong-rung approximation as open diamonds.

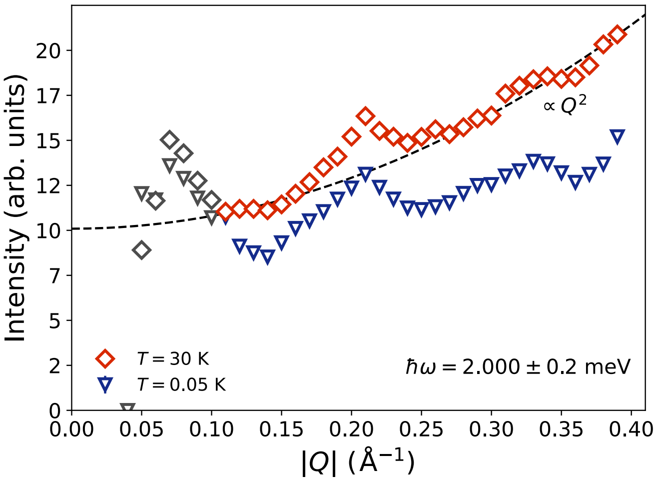

FIG. 11. Phononic character of local modes. Intensity of the vibrational modes obtained by integration over their full energy range and shown at two temperatures as a function of $|Q|$ to reveal conventional phononic behavior, excluding the possibility of a residual magnetic signal at these energies and temperatures. Gray symbols mark data excluded from the $|Q|^2$ fit due to the proximity of detector elements at these small Q values to the direct beam.

$\hbar\omega/J_{\text{leg}}$, and hence work with the reduced parameters Δ/J_{leg}, A/J_{leg}, and B/J_{leg} in Fig. 10. Fitting our Cu-CPA data using the parametrized SMA therefore involves the additional step of reintroducing the energy scale, J_{leg}, as a free parameter. By deducing the two ratios α_a and α_b from our experimental data and extracting the two energy units $J_{\text{leg},a}$ and $J_{\text{leg},b}$, we compute the two rung interactions $J_{\text{rung},a}$ and $J_{\text{rung},b}$ and hence obtain the Heisenberg terms reported in Sec. III B as the complete description of the Cu-CPA system.

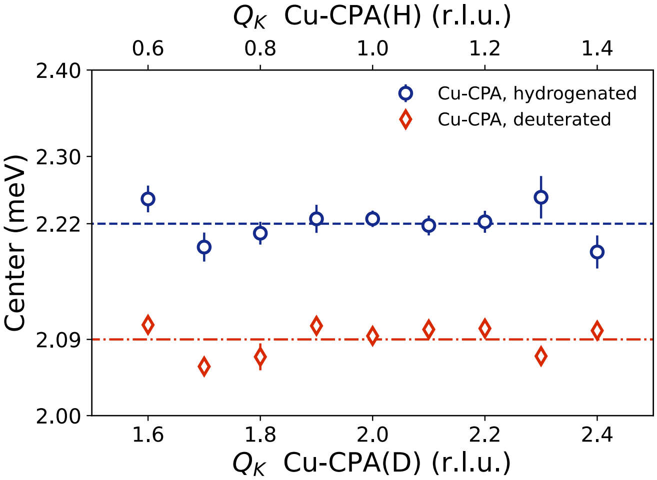

FIG. 12. Isotope effect on the energies of local phonons. Fitted center position of the set of phonon modes appearing around 2.0 meV, shown as a function of Q_K to verify its dispersionless nature. Blue circles show data for the hydrogenated Cu-CPA sample and red diamonds data for a deuterated one. The Cu-CPA(H) dataset was measured on LET and the Cu-CPA(D) dataset on IN5, both at 30 K. The horizontal lines mark the mean energies of the ensemble of local phonons in each sample.

TABLE III. Mass summary for undeuterated, partially deuterated, and fully deuterated CPA molecules, with the mass ratio $m^* = \sqrt{m_{\text{CPA}}^{(\text{X})}/m_{\text{CPA}}^{(\text{H})}}$ shown in the right-hand column.

Atom	Occurrence	Mass (g/mol)	Total mass	m^*
C	5	12.011	60.055	
H	9	1.007	9.063	
N	1	14.007	14.007	
H	3	1.007	3.021	
Total			*86.146*	1.000
C	5	12.011	60.055	
D	9	2	18	
N	1	14.007	14.007	
H	3	1.007	3.021	
Total			*95.083*	1.051
C	5	12.011	60.055	
D	9	2	18	
N	1	14.007	14.007	
D	3	2	6	
Total			*98.062*	1.067

APPENDIX F: PROPERTIES OF THE LOCAL PHONONS

To demonstrate that the flat modes appearing around 2 meV are of phononic origin, we prepared powder averages of the scattering intensity of our deuterated sample by integrating over the energy range 1.8–2.2 meV. As Fig. 11 shows, at 30 K this average exhibits clear $|Q|^2$ behavior, which is an unambiguous statement of its phononic nature.

To demonstrate that these phonons have their origin in the CPA molecules, we performed energy scans at $T = 30$ K over a range of Q_K positions to compare the energies of the local phonon excitations in one hydrogenated and one deuterated sample of Cu-CPA. Because these phonons are nondispersive,

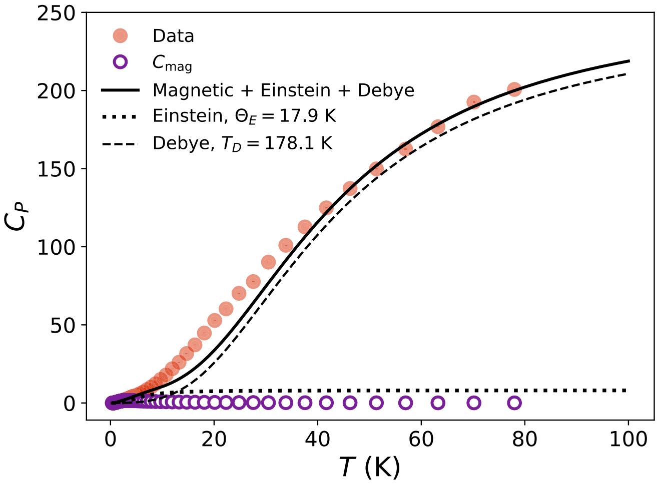

FIG. 13. High-temperature specific heat. Specific-heat measurements of Ref. [24] (red circles) fitted with a model including the magnetic contribution (purple circles), a Debye phononic contribution that accounts for the high-temperature part (dashed line), and an Einstein phononic contribution that accounts for the low-energy local phonons (dotted line). The total of these three contributions is shown by the solid line.

we integrated over all momenta in the perpendicular directions (Q_H and Q_L). The center positions of the phonon modes, determined by fitting a Lorentzian peak with a linear background, are shown in Fig. 12.

Quite generally, the vibrational energy of a molecule is proportional to $1/\sqrt{m}$, where m is the molecular mass. The ratio between the centers of the measured energies is 1.06(1), which is consistent with the square root of the mass ratios of both the partially and fully deuterated CPA molecules listed in Table III. There we show the masses and mass ratios of CPA ligands without deuteration, with full deuteration, and with a partial deuteration where the nine H atoms bonded to C atoms are replaced, but not the three bonded to N atoms (our measured frequencies are not consistent with a 1/4 partial deuteration). Because textbook chemistry indicates that the H atoms are bonded more strongly to C than to N, any deviation from full deuteration would likely indicate that the as-grown samples were very close to being fully deuterated, but lost D atoms on the ammonium groups due to ambient moisture.

APPENDIX G: HIGH-TEMPERATURE SPECIFIC HEAT

In Fig. 13 we show our fit to the specific-heat data reported in Ref. [24] over the full range of available temperatures. We reiterate that the full fit includes the magnetic specific heat computed from the ladder parameters determined by INS, the contribution of low-energy local phonons modeled as Einstein modes (harmonic oscillators), and a generic phonon contribution modeled by fitting a Debye form to the high-temperature regime. The parameters of the two phononic components were fitted recursively. We note the deviation of the full fit from the data between 10 and 30 K, which suggests the influence of further local phonon modes of the CPA units, but avoid the underconstrained exercise of fitting these.

[1] H.-J. Mikeska and A. K. Kolezhuk, One-dimensional magnetism, in *Quantum Magnetism*, edited by U. Schollwöck, J. Richter, D. J. J. Farnell, and R. F. Bishop (Springer, Berlin, 2004), pp. 1–83.

[2] E. Dagotto and T. M. Rice, Surprises on the way from one- to two-dimensional quantum magnets: The ladder materials, Science **271**, 618 (1996).

[3] T. Giamarchi and A. M. Tsvelik, Coupled ladders in a magnetic field, Phys. Rev. B **59**, 11398 (1999).

[4] D. Schmidiger, S. Mühlbauer, A. Zheludev, P. Bouillot, T. Giamarchi, C. Kollath, G. Ehlers, and A. M. Tsvelik, Symmetric and asymmetric excitations of a strong-leg quantum spin ladder, Phys. Rev. B **88**, 094411 (2013).

[5] Z. Hiroi, M. Azuma, M. Takano, and Y. Bando, A new homologous series $Sr_{n-1}Cu_{n+1}O_{2n}$ found in the SrO-CuO system treated under high pressure, J. Solid State Chem. **95**, 230 (1991).

[6] M. Azuma, Z. Hiroi, M. Takano, K. Ishida, and Y. Kitaoka, Observation of a spin gap in $SrCu_2O_3$ comprising spin-1/2 quasi-1D two-leg ladders, Phys. Rev. Lett. **73**, 3463 (1994).

[7] K. Ishida, Y. Kitaoka, K. Asayama, M. Azuma, Z. Hiroi, and M. Takano, Spin gap behavior in ladder-type of quasi-one-dimensional spin $S = 1/2$ System $SrCu_2O_3$, J. Phys. Soc. Jpn. **63**, 3222 (1994).

[8] K. Kojima, A. Keren, G. M. Luke, B. Nachumi, W. D. Wu, Y. J. Uemura, M. Azuma, and M. Takano, Magnetic behavior of the 2-leg and 3-leg spin ladder cuprates $Sr_{n-1}Cu_{n+1}O_{2n}$, Phys. Rev. Lett. **74**, 2812 (1995).

[9] Z. Hiroi and M. Takano, Absence of superconductivity in the doped antiferromagnetic spin-ladder compound (La,Sr)$CuO_{2.5}$, Nature (London) **377**, 41 (1995).

[10] H. Mayaffre, P. Auban-Senzier, M. Nardone, D. Jérome, D. Poilblanc, C. Bourbonnais, U. Ammerahl, G. Dhalenne, and A. Revcolevschi, Absence of a spin gap in the superconducting ladder compound $Sr_2Ca_{12}Cu_{24}O_{41}$, Science **279**, 345 (1998).

[11] R. S. Eccleston, M. Uehara, J. Akimitsu, H. Eisaki, N. Motoyama, and S. I. Uchida, Spin dynamics of the spin-ladder dimer-chain material $Sr_{14}Cu_{24}O_{41}$, Phys. Rev. Lett. **81**, 1702 (1998).

[12] R. D. Willett, C. Galeriu, C. P. Landee, M. M. Turnbull, and B. Twamley, Structure and magnetism of a spin ladder system: $(C_5H_9NH_3)_2CuBr_4$, Inorg. Chem. **43**, 3804 (2004).

[13] Ch. Rüegg, K. Kiefer, B. Thielemann, D. F. McMorrow, V. Zapf, B. Normand, M. B. Zvonarev, P. Bouillot, C. Kollath, T. Giamarchi, S. Capponi, D. Poilblanc, D. Biner, and K. W. Krämer, Thermodynamics of the spin luttinger liquid in a model ladder material, Phys. Rev. Lett. **101**, 247202 (2008).

[14] S. Ward, P. Bouillot, H. Ryll, K. Kiefer, K. W. Krämer, Ch. Rüegg, C. Kollath, and T. Giamarchi, Spin ladders and quantum simulators for Tomonaga–Luttinger liquids, J. Phys.: Condens. Matter **25**, 014004 (2013).

[15] S. Ward, M. Mena, P. Bouillot, C. Kollath, T. Giamarchi, K. P. Schmidt, B. Normand, K. W. Krämer, D. Biner, R. Bewley, T. Guidi, M. Boehm, D. F. McMorrow, and Ch. Rüegg, Bound states and field-polarized haldane modes in a quantum spin ladder, Phys. Rev. Lett. **118**, 177202 (2017).

[16] M. Klanjšek, H. Mayaffre, C. Berthier, M. Horvatić, B. Chiari, O. Piovesana, P. Bouillot, C. Kollath, E. Orignac, R. Citro, and T. Giamarchi, Controlling luttinger liquid physics in spin ladders under a magnetic field, Phys. Rev. Lett. **101**, 137207 (2008).

[17] B. Thielemann, Ch. Rüegg, H. M. Rønnow, A. M. Läuchli, J.-S. Caux, B. Normand, D. Biner, K. W. Krämer, H.-U. Güdel, J. Stahn, K. Habicht, K. Kiefer, M. Boehm, D. F. McMorrow, and J. Mesot, Direct observation of magnon fractionalization in the quantum spin ladder, Phys. Rev. Lett. **102**, 107204 (2009).

[18] B. Wehinger, F. T. Lisandrini, N. Kestin, P. Bouillot, S. Ward, B. Thielemann, R. Bewley, M. Boehm, D. Biner, K. W. Krämer, B. Normand, T. Giamarchi, C. Kollath, A. M. Läuchli, and Ch. Rüegg, Fingerprints of supersymmetric spin and charge dynamics observed by inelastic neutron scattering, Nat. Commun. **16**, 3228 (2025).

[19] D. Schmidiger, S. Mühlbauer, S. N. Gvasaliya, T. Yankova, and A. Zheludev, Long-lived magnons throughout the Brillouin zone of the strong-leg spin ladder $(C_7H_{10}N)_2CuBr_4$, Phys. Rev. B **84**, 144421 (2011).

[20] D. Schmidiger, P. Bouillot, S. Mühlbauer, S. Gvasaliya, C. Kollath, T. Giamarchi, and A. Zheludev, Spectral and thermo-

dynamic properties of a strong-leg quantum spin ladder, Phys. Rev. Lett. **108**, 167201 (2012).

[21] D. Schmidiger, P. Bouillot, T. Guidi, R. Bewley, C. Kollath, T. Giamarchi, and A. Zheludev, Spectrum of a magnetized strong-leg quantum spin ladder, Phys. Rev. Lett. **111**, 107202 (2013).

[22] P. Bouillot, C. Kollath, A. M. Läuchli, M. Zvonarev, B. Thielemann, Ch. Rüegg, E. Orignac, R. Citro, M. Klanjšek, C. Berthier, M. Horvatić, and T. Giamarchi, Statics and dynamics of weakly coupled antiferromagnetic spin-$\frac{1}{2}$ ladders in a magnetic field, Phys. Rev. B **83**, 054407 (2011).

[23] M. Jeong, H. Mayaffre, C. Berthier, D. Schmidiger, A. Zheludev, and M. Horvatić, Magnetic-order crossover in coupled spin ladders, Phys. Rev. Lett. **118**, 167206 (2017).

[24] J. Philippe, F. Elson, N. P. M. Casati, S. Sanz, M. Metzelaars, O. Shliakhtun, O. K. Forslund, J. Lass, T. Shiroka, A. Linden, D. G. Mazzone, J. Ollivier, S. Shin, M. Medarde, B. Lake, M. Månsson, M. Bartkowiak, B. Normand, P. Kögerler, Y. Sassa, *et al.*, $(C_5H_9NH_3)_2CuBr_4$: A metal-organic two-ladder quantum magnet, Phys. Rev. B **110**, 094101 (2024).

[25] J. Lass, H. Jacobsen, K. M. L. Krighaar, D. Graf, F. Groitl, F. Herzog, M. Yamada, C. Kägi, R. A. Müller, R. Bürge, M. Schild, M. S. Lehmann, A. Bollhalder, P. Keller, M. Bartkowiak, U. Filges, U. Greuter, G. Theidel, H. M. Rønnow, C. Niedermayer, *et al.*, Commissioning of the novel continuous angle multi-energy analysis spectrometer at the Paul Scherrer Institut, Rev. Sci. Instrum. **94**, 023302 (2023).

[26] J. Ollivier and H. Mutka, IN5 cold neutron time-of-flight spectrometer, prepared to tackle single crystal spectroscopy, J. Phys. Soc. Jpn. **80**, SB003 (2011).

[27] R. I. Bewley, J. W. Taylor, and S. M. Bennington, LET, a cold neutron multi-disk chopper spectrometer at ISIS, Nucl. Instrum. Meth. A **637**, 128 (2011).

[28] J. Lass, H. Jacobsen, D. G. Mazzone, and K. Lefmann, Mjolnir: A software package for multiplexing neutron spectrometers, SoftwareX **12**, 100600 (2020).

[29] R. A. Ewings, A. Buts, M. D. Le, J. van Duijn, I. Bustinduy, and T. G. Perring, Horace: Software for the analysis of data from single crystal spectroscopy experiments at time-of-flight neutron instruments, Nucl. Instrum. Meth. Phys. Res. A **834**, 132 (2016).

[30] T. Barnes, E. Dagotto, J. Riera, and E. S. Swanson, Excitation spectrum of Heisenberg spin ladders, Phys. Rev. B **47**, 3196 (1993).

[31] H. Krull, N. A. Drescher, and G. S. Uhrig, Enhanced perturbative continuous unitary transformations, Phys. Rev. B **86**, 125113 (2012).

[32] T. Barnes and J. Riera, Susceptibility and excitation spectrum of $(VO)_2P_2O_7$ in ladder and dimer-chain models, Phys. Rev. B **50**, 6817 (1994).

[33] S. Bettler, G. Simutis, G. Perren, D. Blosser, S. Gvasaliya, and A. Zheludev, High-pressure Raman study of the quantum magnet $(C_4H_{12}N_2)Cu_2Cl_6$, Phys. Rev. B **96**, 174431 (2017).

[34] S. Bettler, L. Stoppel, Z. Yan, S. Gvasaliya, and A. Zheludev, Sign switching of dimer correlations in $SrCu_2(BO_3)_2$ under hydrostatic pressure, Phys. Rev. Res. **2**, 012010(R) (2020).

[35] R. E. Lechner, G. Badurek, A. J. Dianoux, H. Hervet, and F. Volino, On the rotational motion of the ammonium ion in the CsCl-type phase of NH_4Br: Results from quasielastic neutron scattering, J. Chem. Phys. **73**, 934 (1980).

[36] A. G. Seel, E. Zurek, A. J. Ramirez-Cuesta, K. R. Ryan, M. T. J. Lodge, and P. P. Edwards, Low energy structural dynamics and constrained libration of $Li(NH_3)_4$, the lowest melting point metal, Chem. Commun. **50**, 10778 (2014).

[37] T. Hong, Y. H. Kim, C. Hotta, Y. Takano, G. Tremelling, M. M. Turnbull, C. P. Landee, H.-J. Kang, N. B. Christensen, K. Lefmann, K. P. Schmidt, G. S. Uhrig, and C. Broholm, Field-induced tomonaga-luttinger liquid phase of a two-leg spin-1/2 ladder with strong leg interactions, Phys. Rev. Lett. **105**, 137207 (2010).

[38] A. Shapiro, C. P. Landee, M. M. Turnbull, J. Jornet, M. Deumal, J. J. Novoa, M. A. Robb, and W. Lewis, Synthesis, structure, and magnetic properties of an antiferromagnetic spin-ladder complex: Bis(2,3-dimethylpyridinium) tetrabromocuprate, J. Am. Chem. Soc. **129**, 952 (2007).

[39] M. Fechner, A. Sukhov, L. Chotorlishvili, C. Kenel, J. Berakdar, and N. A. Spaldin, Magnetophononics: Ultrafast spin control through the lattice, Phys. Rev. Mater. **2**, 064401 (2018).

[40] F. Giorgianni, B. Wehinger, S. Allenspach, N. Colonna, C. Vicario, P. Puphal, E. Pomjakushina, B. Normand, and Ch. Rüegg, Ultrafast frustration breaking and magnetophononic driving of singlet excitations in a quantum magnet, Phys. Rev. B **107**, 184440 (2023).

[41] B. Demazure, M. Krebs, G. S. Uhrig, and B. Normand, Pulsed magnetophononics in gapped quantum magnets, Phys. Rev. B **112**, 075112 (2025).

[42] F. Elson, O. K. Forslund, Y. Ge, P. Kögerler, B. Lake, M. Mansson, J. Ollivier, R. Palm, J. Philippe, S. Sanz, Y. Sassa, O. Shliakhtun, and G. Simutis, Magnetic excitations in a quantum spin ladder $(C_5H_9NH_3)_2CuBr_4$, Institut Laue-Langevin (ILL) (2023), https://dx.doi.org/10.5291/ILL-DATA.4-05-849.

[43] J. Philippe, T. Arh, F. Elson, N. Hollmann, M. Janoschek, C. Y. Jiang, P. Kögerler, M. Mansson, M. Metzelaars, J. Ollivier, Y. Sassa, G. Simutis, and D. W. Tam, Symmetric mode in the double ladder Cu-CPA, Institut Laue-Langevin (ILL) (2025), https://dx.doi.org/10.5291/ILL-DATA.4-05-927.

[44] G. Simutis, M. Mansson, Y. Sassa, B. Lake, J. Philippe, C. Balz, M. Janoschek, F. Elson, and R. Stewart, Magnetic excitations in a quantum spin ladder $(C_5H_9NH_3)_2CuBr_4$, STFC ISIS Neutron and Muon Source (2025), https://doi.org/10.5286/ISIS.E.RB2210245-1.

[45] F. D. M. Haldane, Nonlinear field theory of large-spin Heisenberg antiferromagnets: Semiclassically quantized solitons of the one-dimensional easy-axis Néel state, Phys. Rev. Lett. **50**, 1153 (1983).

[46] A. Auerbach, *Interacting Electrons and Quantum Magnetism* (Springer, New York, 1994).

[47] A. Zheludev, V. O. Garlea, T. Masuda, H. Manaka, L.-P. Regnault, E. Ressouche, B. Grenier, J.-H. Chung, Y. Qiu, K. Habicht, K. Kiefer, and M. Boehm, Dynamics of quantum spin liquid and spin solid phases in IPA-$CuCl_3$ under an applied magnetic field studied with neutron scattering, Phys. Rev. B **76**, 054450 (2007).

[48] D. Schmidiger, K. Y. Povarov, S. Galeski, N. Reynolds, R. Bewley, T. Guidi, J. Ollivier, and A. Zheludev, Emergent interacting spin islands in a depleted strong-leg Heisenberg ladder, Phys. Rev. Lett. **116**, 257203 (2016).

[49] M. Reigrotzki, H. Tsunetsugu, and T. M. Rice, Strong-coupling expansions for antiferromagnetic Heisenberg spin-one-half ladders, J. Phys.: Condens. Matter **6**, 9235 (1994).